

Size matters: are we witnessing super-Eddington accretion in high-redshift black holes from JWST?

Alessandro Lupi^{1,2,*}, Alessandro Trinca¹, Marta Volonteri³, Massimo Dotti^{4,2}, and Chiara Mazzucchelli⁵

¹ Dipartimento di Scienza e Alta Tecnologia, Università degli Studi dell’Insubria, via Valleggio 11, I-22100, Como, Italy

² INFN, Sezione di Milano-Bicocca, Piazza della Scienza 3, I-20126 Milano, Italy

³ Institut d’Astrophysique de Paris, UMR 7095, CNRS and Sorbonne Université, 98 bis boulevard Arago, 75014 Paris, France

⁴ Dipartimento di Fisica “G. Occhialini”, Università degli Studi di Milano-Bicocca, Piazza della Scienza 3, I-20126 Milano, Italy

⁵ Instituto de Estudios Astrofísicos, Facultad de Ingeniería y Ciencias, Universidad Diego Portales, Avenida Ejército Libertador 441, Santiago, Chile

Draft June 27, 2024

ABSTRACT

Observations by the James Webb Space Telescope of the Universe at $z \gtrsim 4$ have shown that massive black holes (MBHs) appear extremely overmassive compared to the local correlation for active galactic nuclei. In some cases, these objects might even reach half the stellar mass inferred for the galaxy. Understanding how such objects formed and grew to this masses has then become a big challenge for theoretical models, with different ideas ranging from heavy seed to super-Eddington accretion phases. Here, we take a different approach, and try to infer how accurate these MBH mass estimates are and whether we really need to revise our physical models. By considering how the emerging spectrum (both the continuum and the broad lines) of an accreting MBH changes close to and above the Eddington limit, we infer a much larger uncertainty in the MBH mass estimates relative to that of local counterparts, up to an order of magnitude, and a potential preference for lower masses and higher accretion rates, which i) move them closer to the local correlations, and ii) might indicate that we are witnessing for the first time a widespread phase of very rapid accretion.

Key words. accretion disks - black hole physics - galaxies: active - galaxies: high-redshift

1. Introduction

Massive black holes (MBHs) are ubiquitously found to inhabit the centre of massive galaxies up to redshift $z \gtrsim 6$ (e.g. Fan et al. 2006; Mortlock et al. 2011; Bañados et al. 2018; Fan et al. 2023; Maiolino et al. 2023), with masses in the range $\sim 10^5 - 10^{10} M_{\odot}$. Observationally, they are commonly identified via gas accretion through the conversion of gravitational energy into radiation, which makes them shine as Active Galactic Nuclei (AGN). They sometimes also produce powerful collimated jets.

MBHs are expected to gain most of their mass via radiatively efficient accretion (Soltan 1982; Marconi et al. 2004), hence they should have formed from lower-mass black hole ‘seeds’ (see, e.g., Inayoshi et al. 2020 and Volonteri et al. 2021 for a review).

With the advent of the James Webb Space Telescope (JWST), we have pushed the observational limit deeply in the dark ages, finding galaxies up to $z \sim 14$ (Carniani et al. 2024). Some of these galaxies also hosted MBHs, which appear to challenge most MBH formation mechanisms, unless one assumes an initially heavy seed ($10^4 - 10^5 M_{\odot}$) and a continuous growth at the Eddington limit. Theoretical models are further challenged by the large abundance of these (candidate) objects (e.g. Harikane et al. 2023; Maiolino et al. 2023; Greene et al. 2024), which implies a formation efficiency of massive seeds way larger than what found in theoretical models. Several studies have shown that this issue can be alleviated if one considers the plausibility of accretion above the Eddington limit (e.g., Lupi et al. 2016; Pezzulli et al. 2016; Regan et al. 2019; Massonneau et al. 2023; Lupi et al. 2023; Shi et al. 2024), which can

compensate for the stunted growth in low-mass galaxies (see, e.g. Anglés-Alcázar et al. 2017). Apart from the mass of these MBHs, another important difference with the local population is that these MBHs seem to be extremely massive compared to their galaxy hosts, lying well above the local correlations (Farina et al. 2022; Maiolino et al. 2023; Yue et al. 2024; Stone et al. 2024) in some cases even weighing more than half the total stellar mass (Juodžbalis et al. 2024). Note, however, that an important role in the comparison is also played by the galaxy mass employed, either the stellar mass, as in the recent JWST results, or the dynamical mass, as in the case of ALMA observations (Decarli et al. 2018; Izumi et al. 2021; Farina et al. 2022). Among the theoretical efforts to explain these systems, the most promising solutions consider i) a somewhat extremely efficient heavy seed formation at high redshifts and an efficient suppression of star formation by the accreting MBH, ii) a strong observational bias (Li et al. 2024), or iii) a population of primordial MBHs (Ziparo et al. 2022; Dolgov 2024). Despite these efforts, a clear consensus is still missing to date, partially because of the large uncertainties in the stellar mass and (potentially) in the MBH mass. This second possibility is rarely considered. In fact, the MBH mass at these redshifts is commonly inferred through the single-epoch method, employing the virial theorem combined with the correlations between the broad $H\alpha$, $H\beta$, or $MgII$ line widths and luminosities, and the emission properties of the continuum emitted by the innermost regions of the accretion disc. These correlations have been calibrated in the local Universe ($z \lesssim 0.3$ Vestergaard & Osmer 2009; Bentz et al. 2013; Reines et al. 2013; Reines & Volonteri 2015), and then extrapolated at high redshift.

* alessandro.lupi@uninsubria.it

Recently, King (2024) pointed out that close-to-Eddington or super-Eddington accreting MBHs would have (i) the emission from the accretion disc beamed by multiple scatterings within the funnel created by a central thickening of the disc itself and (ii) unvirialized BLR whose dynamics is mostly dominated by outflows. Under such conditions, King (2024) demonstrated that the MBH estimates inferred would be artificially biased towards high values, and argued that such an effect might be particularly relevant for high-redshift AGN. Another potential source of bias could instead result from an inaccurate estimate of the broad line region (BLR) size, as suggested by recent reverberation mapping campaigns - including the SEAMBH (Du et al. 2014) and the SDSS-RM (Grier et al. 2017) - of multiple highly accreting MBHs, Martínez-Aldama et al. (2019).

In particular, these campaigns demonstrated that the time lag of the H β line, which is directly associated to the size of the BLR, depends on the accretion rate of the MBH, and shortens for accretion rates above $f_{\text{Edd}} \sim 0.3$ (Wang et al. 2014, W14 hereafter). The proposed interpretation for such effect is radiation pressure which, for accretion rates close and above the Eddington limit, thickens the accretion disc. Such a thicker disc is better described by the slim-disc solution (Abramowicz et al. 1988) rather than by a more standard radiatively efficient Shakura & Sunyaev (1973, SS hereafter) disc, and results in a lower flux of ionizing photons reaching the BLR clouds compared to a radiatively efficient AGN with identical optical spectrum. In these conditions, the BLR splits in unshadowed and shadowed regions, the latter receiving less photons and shrinking in size, which result in a net shorter lag.

Motivated by these results, in this work we explore the effect of a varying BLR size, based on the aforementioned results and on a fully physical approach, on the inferred MBH masses in the most challenging high-redshift sources observed by JWST to date. In particular, we account for the possibility that the observed luminosities might be the result of a lower mass, highly accreting MBH, with the aim of assessing potential biases in the MBH mass estimates.

The manuscript is organised as follows. In Section 2 we describe our procedure to estimate the MBH mass, in Section 3 we present our results, and in Section 4 we discuss potential caveats in the analysis and draw our conclusions.

2. Methods

In order to test how relevant the evolution of the BLR size with the Eddington ratio is in high-redshift systems, we build a theoretical model of the accretion disc and the BLR emissions based on the electromagnetic spectrum of a slim disc, as defined by the AGNSLIM model in XSPEC (Kubota & Done 2019). Of the many parameters available in the model, in our work we only considered the impact of the three main ones: the MBH mass M_{BH} , the Eddington ratio $L_{\text{thin}}/L_{\text{Edd}} \equiv \eta_{\text{thin}} \dot{M}_{\text{BH}} c^2 / L_{\text{Edd}}$, with L_{thin} and η_{thin} being the bolometric luminosity and the radiative efficiency of a SS disc, and the MBH spin a_{BH} , leaving the others to their default value. We sample 6250 different combinations, with 25 logarithmically-spaced MBH masses between 10^5 and $10^{10} M_{\odot}$, 25 logarithmically-spaced Eddington ratios in the range $0.01 - 10^3$, and 10 linearly-spaced values of the MBH spin between 0 and 0.998. The spectrum covers the energy range 0.1 eV – 100 keV, corresponding to a wavelength range $0.12 \text{ \AA} - 12.4 \mu\text{m}$, in 1000 logarithmically-spaced bins.

After the spectra have been generated, for each combination we tabulate the luminosity at 5100 \AA (L_{5100}), and the ionising luminosity L_{ion} above $E > 0.1 \text{ keV}$ (soft-X; Kwan & Krolik 1979),

the latter needed to determine the broad-line emission from the disc properties (see, e.g. Osterbrock & Ferland 2006). For consistency with Kubota & Done (2019), we normalize the spectrum bolometric luminosity to the value estimated from the numerical integration of the slim disc solution by Sadowski (2011). This normalisation allows gives us the effective radiative efficiency η for each combination of the three model parameters, that we use in the rest of the paper to determine $L/L_{\text{Edd}} = \eta/\eta_{\text{thin}} L_{\text{thin}}/L_{\text{Edd}}$. With the table so created, we then built a theoretical model for the BLR emission to be compared with observations. In particular, the observed quantities we considered are: the broad-line width (either H α or H β) and the luminosity (either the H α luminosity or the luminosity at 5100 \AA), according to the values reported in the corresponding observational works (Harikane et al. 2023; Maiolino et al. 2023; Übler et al. 2023; Greene et al. 2024), both with their associated uncertainties σ .

Our model is defined as follows.

- Given a specific combination of M_{BH} , $L_{\text{thin}}/L_{\text{Edd}}$ and a_{BH} , we extract $L_{5100 \text{ \AA}}$ and L_{ion} via tri-linear interpolation on our table.
- For simplicity, we do not make any specific assumption on the cloud properties in the BLR, and generically assume that they are homogeneously distributed around the central MBH (Wang et al. 2014).¹ Following W14, we assume that self-shadowing is negligible within the funnel, which is defined by an aperture

$$\theta_{\text{fun}} \approx \begin{cases} 90^\circ & f_{\text{Edd}} < 8 \\ 118^\circ - 33^\circ \log f_{\text{Edd}} & 8 \geq f_{\text{Edd}} < 100 \\ 76^\circ - 12^\circ \log f_{\text{Edd}} & f_{\text{Edd}} \geq 100 \end{cases}, \quad (1)$$

where $f_{\text{Edd}} \equiv \dot{M}_{\text{BH}} c^2 / L_{\text{Edd}} = \eta_{\text{thin}}^{-1} L_{\text{thin}} / L_{\text{Edd}}$, and that the ionising radiation emitted within this solid angle directly impinges on the BLR clouds. Assuming an intrinsic spectrum with angular distribution $dF/d\theta \propto \cos \theta$, we then determine the broad-line emission from clouds within the funnel solid angle assuming the local correlation (Greene & Ho 2005)

$$\frac{L_{\text{H}\beta, \text{fun}}}{10^{42} \text{ erg s}^{-1}} = (1.425 \pm 0.007) \left(\frac{x_{\text{fun}} L_{5100 \text{ \AA}}}{10^{44} \text{ erg s}^{-1}} \right)^{1.133 \pm 0.005}, \quad (2)$$

where x_{fun} is the fraction of the total ionising flux within the funnel. Outside the funnel, instead, we model self-shadowing through Eq. (19) in W14

$$\frac{L_{\text{H}\beta, \text{s-s}}}{L_{\text{H}\beta, \text{fun}}} \approx 0.28 \frac{\xi_{\text{s-s}}}{\xi_{\text{fun}}} \frac{\cos \theta_{\text{fun}}}{1 - \cos \theta_{\text{fun}}} \left(\frac{f_{\text{Edd}}}{50} \right)^{-0.6}, \quad (3)$$

where $\xi_{\text{s-s}}$ and ξ_{fun} are the anisotropic factors for H β emission from the BLR clouds in the self-shadowed region and within the funnel respectively. As these values are completely unconstrained, but for pole-on observers (where they are both equal to unity). Here, we assume for simplicity that they are always of the same order and remove them from the equation. The total H β luminosity is finally estimated as $L_{\text{H}\beta} = L_{\text{H}\beta, \text{fun}} + L_{\text{H}\beta, \text{s-s}}$.

¹ This is a very simplistic assumption, as both the cloud angular distribution and their maximum distance from the source are completely unconstrained. Previous studies hinted at a common disc-like geometry for the BLR (e.g. Wills & Browne 1986; Collin-Souffrin 1987; Runnoe et al. 2013). We stress that a flatter BLR would enhance the self-shadowing effect.

In order to determine the $H\alpha$ luminosity, we assume the standard scaling from Greene & Ho (2005)

$$\frac{L_{H\alpha}}{10^{42} \text{ erg s}^{-1}} = (5.25 \pm 0.02) \left(\frac{L_{5100\text{\AA},\text{proxy}}}{10^{44} \text{ erg s}^{-1}} \right)^{1.157 \pm 0.005}, \quad (4)$$

where

$$\frac{\tilde{L}_{5100\text{\AA},\text{proxy}}}{10^{44} \text{ erg s}^{-1}} = \left(\frac{L_{H\beta}}{(1.425 \pm 0.007) \times 10^{42} \text{ erg s}^{-1}} \right)^{1/(1.133 \pm 0.005)}. \quad (5)$$

We note that, when the broad-line flux or luminosity are not reported, as in the case of Yue et al. (2024), we directly compare $L_{5100\text{\AA}}$ from our model with the observed data.

- The last piece of information we need for the model is the full-width-half-maximum ($FWHM$) of the broad lines, which we determine by assuming virial equilibrium in the BLR, which gives

$$FWHM_{H\beta} = \sqrt{\frac{R_{\text{BLR}}}{f_{\text{virial}} GM_{\text{BH}}}} \quad (6)$$

for the $H\beta$ line, where f_{virial} is a parameter taking into account the unknown inclination, geometry, and kinematics of the BLR. In this work, we consider as our ‘fiducial’ case $f_{\text{virial}} = 1.075$ (Reines & Volonteri 2015), but also explore a case in which $f_{\text{virial}} \propto (FWHM_{\text{line,obs}})^{-k}$ (Mejía-Restrepo et al. 2018, MR18 hereafter), with $k = 1$ ($H\alpha$) or $k = 1.17$ ($H\beta$). In order to estimate R_{BLR} , we employ the relations derived by Martínez-Aldama et al. (2019)

$$\log \frac{R_{\text{BLR}}}{R_{\text{BLR,Ref}}} = \alpha \log f_{\text{Edd}} + \beta, \quad (7)$$

which takes into account the self-shadowing of the BLR. For the fiducial model, we set $\alpha = -0.143$, $\beta = -0.136$, and assume $R_{\text{BLR,Ref}}$ as the reference $H\beta$ BLR size estimate by Bentz et al. (2013)

$$\log \frac{R_{\text{BLR,Ref}}}{1 \text{ lt} - \text{day}} = 1.527 \pm 0.31 + 0.533_{-0.033}^{+0.035} \log \frac{L_{5100\text{\AA}}}{10^{44} \text{ erg s}^{-1}}. \quad (8)$$

In the MR18 case, we employ instead $\alpha = -0.283$, $\beta = -0.228$, and $f_{\text{Edd}} = f_{\text{virial}}^{-2} \eta_{\text{thin}}^{-1} L_{\text{thin}}/L_{\text{Edd}}$. For sources where the MBH mass is estimated from the $H\alpha$, we finally convert $FWHM_{H\beta}$ to the $FWHM_{H\alpha}$ through the Bentz et al. (2013) relation

$$FWHM_{H\beta} = (1.07 \pm 0.07) \times 10^3 \left(\frac{FWHM_{H\alpha}}{10^3 \text{ km s}^{-1}} \right) \text{ km s}^{-1}. \quad (9)$$

In order to compare our model predictions with observations, we employ a Markov-Chain Monte Carlo (MCMC) algorithm as implemented in the `emcee` package (Foreman-Mackey et al. 2013). We consider here as our observational sample the sources identified by Harikane et al. (2023); Maiolino et al. (2023); Yue et al. (2024); Übler et al. (2023), and Greene et al. (2024), in the redshift range $4 \leq z \leq 7$. The likelihood \mathcal{L} for the MCMC is defined through

$$\ln \mathcal{L} = -\frac{1}{2} \sum_i \left[\frac{(Y_i - \tilde{Y}_i)^2}{s_i^2} + \ln(2\pi s_i^2) \right], \quad (10)$$

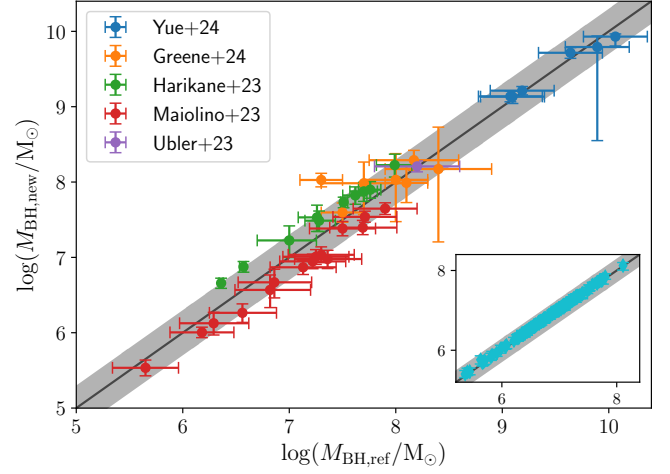


Fig. 1. M_{BH} estimates from the MCMC for the validation run against the MBH mass reported in the observational studies considered in this work. The black line corresponds to the 1:1 relation, with the grey shaded area 0.3 dex wide. The dots correspond to the MBHs in Yue et al. (2024, blue), Greene & Ho (2005, orange), Harikane et al. (2023, green), Maiolino et al. (2023, red), and Übler et al. (2023, purple). In the inset we show the results obtained for the Reines & Volonteri (2015) data as cyan crosses.

where Y_i is the observed broad-line $FWHM$ and the luminosity, \tilde{Y}_i is the value predicted by our model, and s_i is the uncertainty in the observed data (assumed Gaussian). The parameters of our model that we aim at constraining are M_{BH} , $L_{\text{thin}}/L_{\text{Edd}}$, and a_{BH} . As priors, we assume a log-flat distribution for M_{BH} and $L_{\text{thin}}/L_{\text{Edd}}$ over the intervals $[5, 10]$ and $[-3, 3]$ respectively, and a uniform distribution for a_{BH} between 0 and 0.998. We ran the MCMC for 10000 steps employing 32 walkers.² In order to incorporate the uncertainties in the correlations used by our model, every time we employ one of the relations above, we sample the slope and normalisation from a Gaussian distribution centred on the best-fit value and with σ defined by the uncertainty of the fit.³ This choice ensures a proper coverage of the parameter space, even with a very limited dataset given by only two values. In the case of a $FWHM$ -dependent virial factor, we randomly sample the virial factor for each source before starting the MCMC from a Gaussian distribution centred on the observed broad-line $FWHM$ with the observed uncertainty, and keep it constant throughout the optimisation procedure, in line with the correlation found by Mejía-Restrepo et al. (2018).

3. Results

3.1. Model validation

Before running the MCMC with the fiducial model described in the previous section, we decided to validate our procedure by neglecting the effects due to the accretion disc transition to a slim-disc. In practice: i) we employed

$$\log \frac{R_{\text{BLR}}}{1 \text{ lt} - \text{day}} = 1.555 \pm 0.31 + 0.542_{-0.033}^{+0.035} \log \frac{L_{5100\text{\AA}}}{10^{44} \text{ erg s}^{-1}} \quad (11)$$

² The number of steps chosen corresponds to about 100 autocorrelation time-scales, which is sufficient to guarantee a robust optimisation.

³ When the uncertainties are asymmetric, we approximate the distribution as a Gaussian distribution with σ_{eff} the average between the two uncertainties.

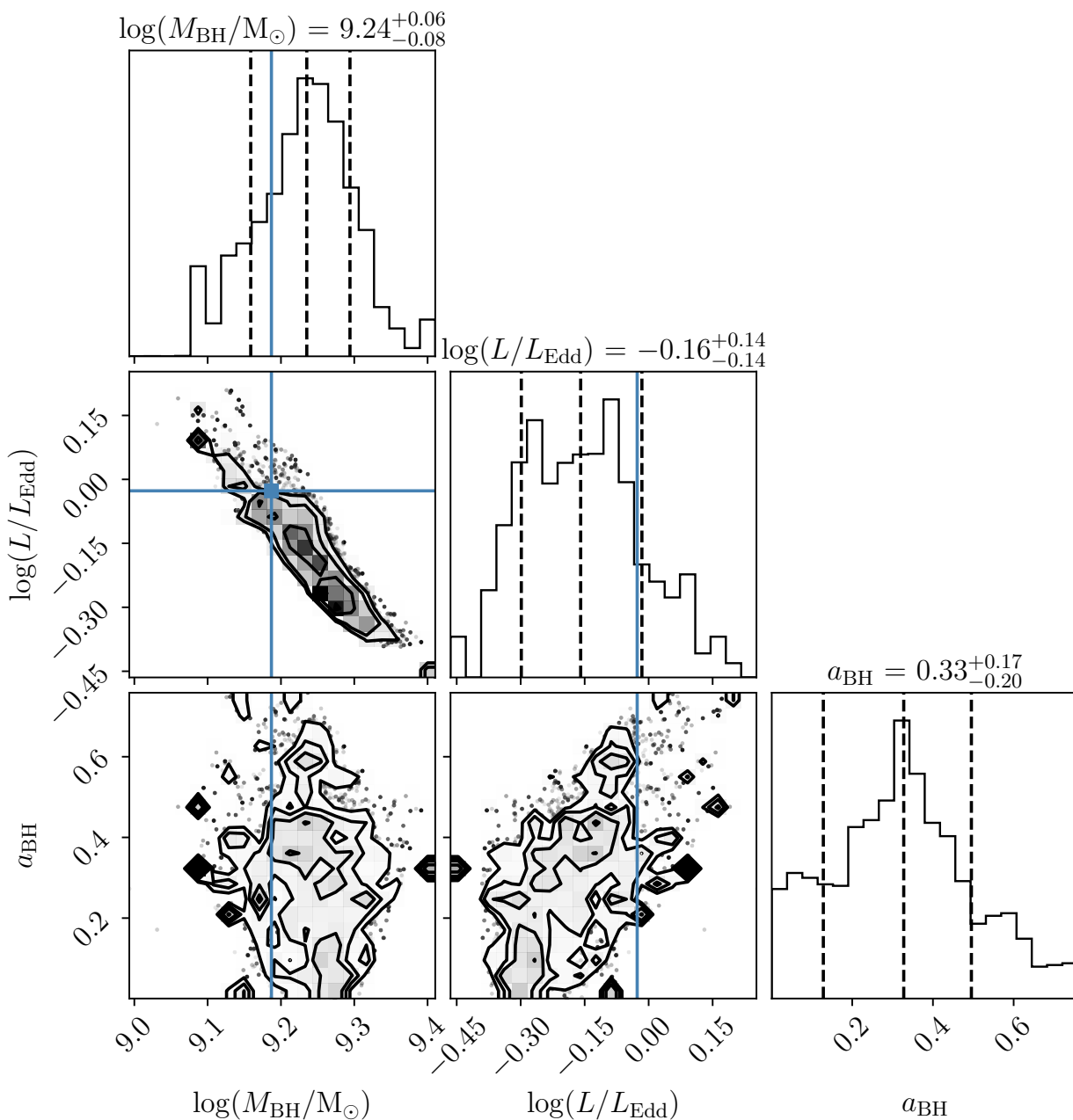


Fig. 2. Corner plot resulting from the MCMC validation run on J1030+0524 (Yue et al. 2024) for the three physical parameters of the model M_{BH} , L/L_{Edd} (obtained by rescaling $L_{\text{thin}}/L_{\text{Edd}}$ as described in Section 2), and a_{BH} . The blue lines correspond to the values reported in the original work.

in Eq. (6), as done in Reines & Volonteri (2015), ii) we inferred the broad-line luminosities from the scaling relations in Bentz et al. (2013, see also Eq.s 2 and 4), using our tabulated value for $L_{5100\text{\AA}}$, and iii) we assumed a constant $f_{\text{virial}} = 1.075$ as in Reines & Volonteri (2015). With these assumptions, we found our best parameters to be in line with those in the published works, as shown in Fig. 1. The inset shows the remarkable agreement of our procedure with the data by Reines & Volonteri (2015). The only mild discrepancy is in the data by Greene et al. (2024), where the estimates show a somewhat larger scatter around the 1:1 relation. The systematic small shift of the Harikane et al. (2023, above) and Maiolino et al. (2023, below) is likely related to the information provided in the respective papers. Maiolino et al. (2023) report the $H\alpha$ flux, which is then converted into

luminosity assuming the cosmology and redshift reported in the discovery paper, while Harikane et al. (2023) give directly the broad line luminosity. We will refer to the MBH masses obtained with this procedure as ‘validation’ in the following.

In general, we find that the spin is very poorly constrained by our MCMC, due to the limited amount of observational data we have and the moderate dependence on its value, whereas the MBH mass and L/L_{Edd} are typically well determined. As an example of the robustness of our procedure, we report in Fig. 2 the corner plot obtained for J1030+0524 from Yue et al. (2024), one of the most massive sources in the sample, which is also one of the few validation cases in which the posterior distribution of the MBH spin exhibits a peak rather than being almost flat. The

blue lines in the corner plot correspond to the estimates from the literature, which agree well with our estimate.

3.2. Full model

In the left panel of Fig. 3, we show the same plot of Fig. 1, but for the slim-disc model. We clearly observe that the fiducial case is close to the 1:1 relation, but typically offset of about 0.5 dex towards lower values compared to those reported in the literature, with correspondingly higher accretion rates, often super-Eddington. The MR18 case, because of the additional dependence of the virial factor on the broad-line *FWHM*, results in even lower MBH masses. The $\dot{M}/\dot{M}_{\text{Edd}}$ ratio is shown in the right panel, where $\dot{M}_{\text{Edd}} \equiv 10L_{\text{Edd}}/c^2$, assuming the fiducial and the MR18 cases of our slim-disc model (red dots and purple squares respectively) and the validation run (black crosses). Despite the differences in the two slim-disc models, we find that the distribution of Eddington ratios is quite similar, with the least massive MBHs more often preferring higher accretion rates. The MR18 case, consistently with the lower MBH masses reported in the left panel, almost always prefer super-Eddington rates, with values between 10 and a 100 times Eddington. Interestingly, the most massive MBHs from Yue et al. (2024) also prefer super-Eddington accretion rates, well above the Eddington limit, which might hint at an ineffective self-regulation of their growth via feedback processes. Another interesting aspect is that, even in the validation run, some MBHs seem to lie above the Eddington limit, especially those with the lowest masses, suggesting that the estimate of their properties according to the local correlations might be biased towards higher MBH masses. Finally, note that discriminating such high accretion rates from more typical cases is not easy, as the luminosity of these objects would never exceed, even in the most extreme cases, a few times the Eddington luminosity (5-10).

As already discussed above, also with slim-disc model, the MBH and the Eddington ratio in our analysis are typically constrained within one order of magnitude, whereas the MBH spin is almost always uniformly distributed, which suggests that our model can accommodate the observed data almost independently of the spin. At super-Eddington rates this is expected, as the effective radiative efficiency does not depend on the spin (Madau et al. 2014). Below the Eddington limit, instead, this suggests that the information available is not sufficient to actually disentangle the spin from the other two parameters.

Finally, we can assess how the correlations between MBHs and their hosts would change considering the results of our full model. The results are shown in Fig. 4, for the fiducial case (left panel) and the MR18 one (right panel). We can observe that our estimates are closer to the local relations, and this effect is more relevant for the MR18 case. Interestingly, this decrease does not completely realign the MBHs with the local correlations, but suggests that the current estimates, especially for the lowest mass MBHs observed, could have a much larger uncertainties than reported in the literature, and their overmassiveness relative to the host should be considered in the light of what we found in this work, besides observational biases.

Even though not reported here, as an estimate of the stellar mass is not available, we performed our analysis also on the sources by Matthee et al. (2024), finding similar variations in the MBH mass to those just discussed. In order to check whether the inclusion of a slim disc emission produced a rigid shift of the MBH masses also for the local sources, we reanalysed the Reines & Volonteri (2015) sample using our fiducial model. We found that, on average, a decrease in the inferred MBH mass was also

present in the local AGN sample, but with variations not larger than 0.2 dex, about a factor of 3 smaller than the intrinsic uncertainty by Reines & Volonteri (2015), and typically much smaller than the 0.5 dex found in the high-redshift sample.

3.3. AGN spectra

As a final check of our procedure, we built synthetic MBH emission spectra for the analysed sources employing all of the three models considered in this work. The best parameters to build the spectra are defined as the average among the 10 evaluations of our MCMC with the maximum likelihood. For each model, we extracted the continuum spectrum from our tables and added on top the emission of the broad line (but for the sources in Yue et al. 2024, where we employed the luminosity at 5100Å). In order to consistently compare with observed spectra, we also accounted for dust extinction following the attenuation law by Calzetti et al. (2000), assuming $R_V = 4.05$ for the source by Harikane et al. (2023), and the Small Magellanic Cloud value $R_V = 2.74$ for the sources by Maiolino et al. (2023) and Greene et al. (2024), to be consistent with the assumptions in the different studies. For the sources observed by the EIGER program (Yue et al. 2024) we did not include any attenuation. The results are reported in Fig. 5 for 4 selected sources: CEERS_02782 (Harikane et al. 2023), JADES_000954 (Maiolino et al. 2023), J0100+2802 (Yue et al. 2024), and UNCOVER_13821 (Greene et al. 2024). We clearly see that our models can always recover the spectral properties of the sources, both the continuum region and the broad H α line intensity and width, independently of the assumptions. The only peculiar case is J0100+2802, where the complexity of the broad H β line profile, not symmetric and with potential hints of offset components, together with the missing modelling of the Iron emission in our model, does not allow us to recover the exact spectrum. Nonetheless, we find that our model very well reproduces the power-law continuum, but for a mildly higher normalisation, simply due to the use in our MCMC of the total continuum luminosity reported in Yue et al. (2024) instead of the contribution of the power-law component only.⁴ This confirms i) the robustness of our procedure, and ii) that the dependence of the BLR emission on the accretion disc structure and the Eddington ratio is somewhat degenerate, resulting in potentially significant differences in the MBH mass estimate if not properly taken into account.

4. Discussion and conclusions

In this work, we have built a semi-empirical model of the BLR emission of MBHs in different accretion regimes. By combining theoretical models of the emission of thin and slim accretion discs (Kubota & Done 2019) with observed scaling relations at low-redshift which naturally account for different accretion regimes, we have built a versatile model that can be applied to high-redshift sources as those recently observed by JWST.

We have incorporated our model in a MCMC tool that we used to re-analyse some recent candidate MBHs from JWST observations. Our results showed that, in many cases, a super-Eddington accreting MBH is preferred with respect to the standard SS accretion disc, which translates in MBH masses of up to an order of magnitude lower. This is in contrast with local

⁴ As a check, we re-ran our MCMC on J0100+2802 with a 5% lower luminosity at 5100Å (consistent with the expected power-law contribution), and found that with almost identical MBH mass estimates the agreement with the power-law fit was remarkable, as expected.

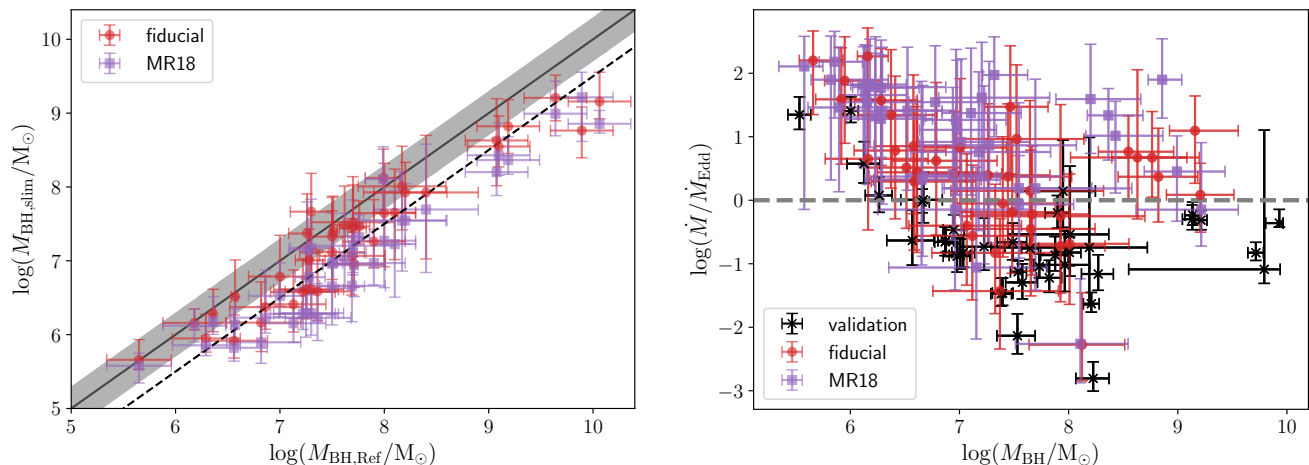


Fig. 3. Left panel: same as Fig. 1, but for our full model, with the estimates of the entire sample shown as red dots (fiducial) and purple squares (MR18). The black dashed line is to guide the eye and corresponds to a 0.5 dex offset relative to the 1:1 relation. Right panel: Eddington ratio distribution for our fiducial model (red dots), the MR18 case (purple squares), and the validation run (black crosses) as a function of the estimated MBH mass. The thick grey dashed line corresponds to the Eddington limit.

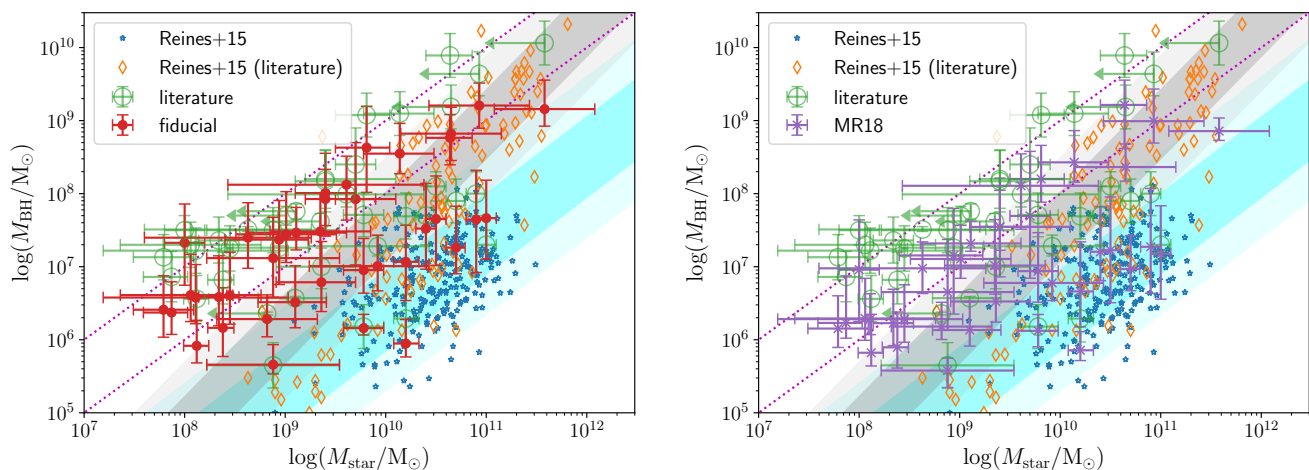


Fig. 4. MBH mass–stellar mass relation for the source in our sample. We show the local AGN from Reines & Volonteri (2015) as blue stars and orange diamonds, with the underlying shaded area correspond to the $1\text{-}\sigma$ and $2\text{-}\sigma$ uncertainties around the best fits to the local samples (grey and cyan for inactive and active galaxies respectively). The original data from the literature is shown as green circles, whereas our new estimates are reported as red dots (left panel) and purple crosses (right panel) for the two virial factors considered. For completeness, we also show as magenta dotted lines constant mass ratios of 0.01 and 0.1.

sources as those by Reines & Volonteri (2015), where more than 95 per cent of the AGN are sub-Eddington and our fiducial model almost perfectly recovers the masses reported in the literature. We also note that the missing detection in X-rays of many of these sources might be compatible with a slim accretion disc, but we leave this aspect to future investigations.

Despite the extreme relevance of potentially detecting and identifying highly super-Eddington sources, the sustainability of this accretion phase over long time-scales is unclear (see, e.g. Regan et al. 2019; Massonneau et al. 2023; Lupi et al. 2023). In particular, there is a potential degeneracy between the MBH mass and the Eddington ratio, and we cannot completely exclude a biased preference for super-Eddington accretion in low-mass systems. In fact, because of the radiation trapping in the innermost regions of the accretion disc, which suppresses the increase in ionising and bolometric luminosity, a slim disc model has more freedom to match the combination of *FWHM* and lumi-

nosities of some of these sources compared to a standard SS disc, without being for this reason more physically plausible. Moreover, any difference in the structure of the BLR (different geometry of the clouds, different density, etc.), as well as different inclinations, might in principle produce similar effects without requiring a highly super-Eddington accretion rate. All these uncertainties enter the virial factor, whose definition can produce variations in the MBH mass estimate up to one order of magnitude, as we have shown here, especially in high-redshift systems for which only a limited amount of information is available.

As for our model, King (2024) pointed out that high-redshift MBH mass estimates could be biased toward too high values. Differently from King (2024), in our analysis we did not consider any radiation beaming nor the possibility that the BLR might be mainly dominated by unvirialized outflows. Considering the more likely super-Eddington nature of many observed sources, and the fact that in these conditions radiation beaming as well

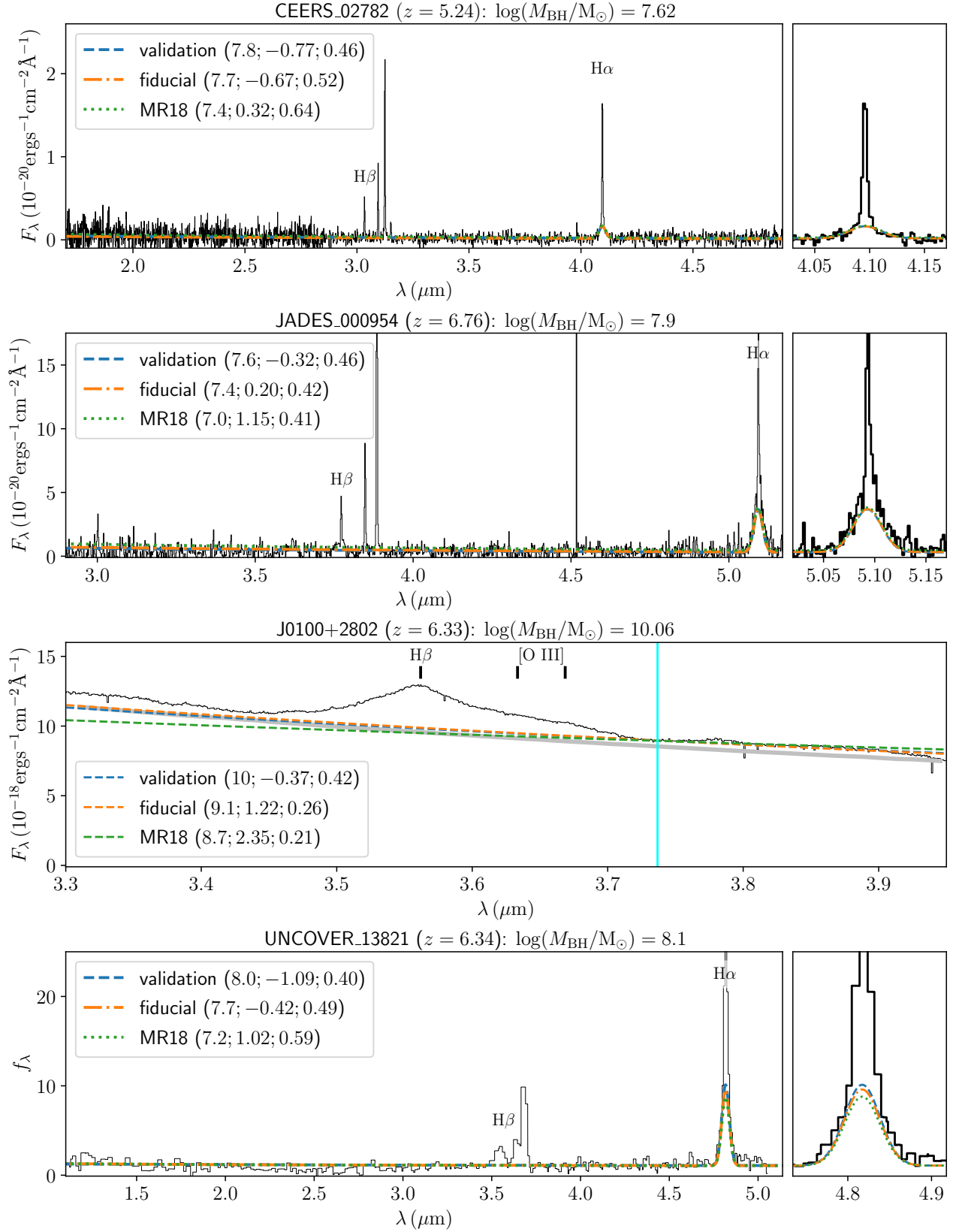


Fig. 5. Reconstructed spectra for 4 selected sources in our sample: CEERS_02782, JADES_000954, J0100+2802, and UNCOVER_13821. The observed spectra (obtained from the public data release of the different programs, but for the UNCOVER source, which has been extracted from the published paper) are shown as black solid lines (with the right panel showing a zoom on the H α line), the blue dashed, orange dash-dotted, and green dotted lines refer to our validation, fiducial, and MR18 models respectively. The cyan vertical line in J0100+2802 corresponds to $\lambda = 5100 \text{ \AA}$ redshifted to the observer frame, which we used to constrain the models. The grey line corresponds to the power-law continuum component from the fit by Yue et al. (2024). All but the UNCOVER source report absolute fluxes, whereas in the UNCOVER case the flux is normalised to the luminosity at 2500 \AA , as done in Greene et al. (2024). The numbers reported in the legend correspond to the parameters employed for each model $\log(M_{\text{MBH}}/M_\odot)$, $\log(L/L_{\text{Edd}})$, and a_{BH} , whereas the mass estimates above each panel correspond to those in the corresponding observational papers.

as nuclear outflows becomes more significant, we expect the uncertainties in the mass estimate to become even larger. Unfortunately, the limited data available does not allow us to confirm whether a bias in the mass is real or not, and whether such a bias might realign MBHs with the local correlation. However, it provides some insights on the impact of detailed accretion disc physics on the MBH mass estimates. In the future, we will incorporate additional information from the observed spectra that will help us to better constrain the actual mass through our physically motivated model.

Acknowledgements. AL and AT acknowledge support from PRIN MUR "2022935STW". AL thanks the organisers of the "Massive black holes in the first billion years" conference Micheal Tremmel and John Regan, as well as Riccardo Beckmann, Amy Reines, and Alberto Sesana for useful discussions that inspired this work.

References

- Abramowicz, M. A., Czerny, B., Lasota, J. P., & Szuszkiewicz, E. 1988, *ApJ*, 332, 646
- Anglés-Alcázar, D., Faucher-Giguère, C.-A., Quataert, E., et al. 2017, *MNRAS*, 472, L109
- Bañados, E., Venemans, B. P., Mazzucchelli, C., et al. 2018, *Nature*, 553, 473
- Bentz, M. C., Denney, K. D., Grier, C. J., et al. 2013, *ApJ*, 767, 149
- Calzetti, D., Armus, L., Bohlin, R. C., et al. 2000, *ApJ*, 533, 682
- Carniani, S., Hainline, K., D'Eugenio, F., et al. 2024, arXiv e-prints, arXiv:2405.18485
- Collin-Souffrin, S. 1987, *A&A*, 179, 60
- Decarli, R., Walter, F., Venemans, B. P., et al. 2018, *ApJ*, 854, 97
- Dolgov, A. D. 2024, arXiv e-prints, arXiv:2401.06882
- Du, P., Hu, C., Lu, K.-X., et al. 2014, *ApJ*, 782, 45
- Fan, X., Bañados, E., & Simcoe, R. A. 2023, *ARA&A*, 61, 373
- Fan, X., Strauss, M. A., Richards, G. T., et al. 2006, *AJ*, 131, 1203
- Farina, E. P., Schindler, J.-T., Walter, F., et al. 2022, *ApJ*, 941, 106
- Foreman-Mackey, D., Hogg, D. W., Lang, D., & Goodman, J. 2013, *PASP*, 125, 306
- Greene, J. E. & Ho, L. C. 2005, *ApJ*, 630, 122
- Greene, J. E., Labbe, I., Goulding, A. D., et al. 2024, *ApJ*, 964, 39
- Grier, C. J., Trump, J. R., Shen, Y., et al. 2017, *ApJ*, 851, 21
- Harikane, Y., Zhang, Y., Nakajima, K., et al. 2023, *ApJ*, 959, 39
- Inayoshi, K., Visbal, E., & Haiman, Z. 2020, *ARA&A*, 58, 27
- Izumi, T., Matsuoka, Y., Fujimoto, S., et al. 2021, *ApJ*, 914, 36
- Juodžbalis, I., Maiolino, R., Baker, W. M., et al. 2024, arXiv e-prints, arXiv:2403.03872
- King, A. 2024, *MNRAS*, 531, 550
- Kubota, A. & Done, C. 2019, *MNRAS*, 489, 524
- Kwan, J. & Krolik, J. H. 1979, *ApJ*, 233, L91
- Li, J., Silverman, J. D., Shen, Y., et al. 2024, arXiv e-prints, arXiv:2403.00074
- Lupi, A., Haardt, F., Dotti, M., et al. 2016, *MNRAS*, 456, 2993
- Lupi, A., Quadri, G., Volonteri, M., Colpi, M., & Regan, J. A. 2023, arXiv e-prints, arXiv:2312.08422
- Madau, P., Haardt, F., & Dotti, M. 2014, *ApJ*, 784, L38
- Maiolino, R., Scholtz, J., Curtis-Lake, E., et al. 2023, arXiv e-prints, arXiv:2308.01230
- Marconi, A., Risaliti, G., Gilli, R., et al. 2004, *MNRAS*, 351, 169
- Martínez-Aldama, M. L., Czerny, B., Kawka, D., et al. 2019, *ApJ*, 883, 170
- Massonneau, W., Volonteri, M., Dubois, Y., & Beckmann, R. S. 2023, *A&A*, 670, A180
- Matthee, J., Naidu, R. P., Brammer, G., et al. 2024, *ApJ*, 963, 129
- Mejía-Restrepo, J. E., Lira, P., Netzer, H., Trakhtenbrot, B., & Capellupo, D. M. 2018, *Nature Astronomy*, 2, 63
- Mortlock, D. J., Warren, S. J., Venemans, B. P., et al. 2011, *Nature*, 474, 616
- Osterbrock, D. E. & Ferland, G. J. 2006, *Astrophysics of gaseous nebulae and active galactic nuclei*
- Pezzulli, E., Valiante, R., & Schneider, R. 2016, *MNRAS*, 458, 3047
- Regan, J. A., Downes, T. P., Volonteri, M., et al. 2019, *MNRAS*, 486, 3892
- Reines, A. E., Greene, J. E., & Geha, M. 2013, *ApJ*, 775, 116
- Reines, A. E. & Volonteri, M. 2015, *ApJ*, 813, 82
- Runnoe, J. C., Shang, Z., & Brotherton, M. S. 2013, *MNRAS*, 435, 3251
- Sadowski, A. 2011, arXiv e-prints, arXiv:1108.0396
- Shakura, N. I. & Sunyaev, R. A. 1973, *A&A*, 24, 337
- Shi, Y., Kremer, K., & Hopkins, P. F. 2024, arXiv e-prints, arXiv:2405.12164
- Soltan, A. 1982, *MNRAS*, 200, 115
- Stone, M. A., Lyu, J., Rieke, G. H., Alberts, S., & Hainline, K. N. 2024, *ApJ*, 964, 90
- Übler, H., Maiolino, R., Curtis-Lake, E., et al. 2023, *A&A*, 677, A145
- Vestergaard, M. & Osmer, P. S. 2009, *ApJ*, 699, 800
- Volonteri, M., Habouzit, M., & Colpi, M. 2021, *Nature Reviews Physics*, 3, 732
- Wang, J.-M., Qiu, J., Du, P., & Ho, L. C. 2014, *ApJ*, 797, 65
- Wills, B. J. & Browne, I. W. A. 1986, *ApJ*, 302, 56
- Yue, M., Eilers, A.-C., Simcoe, R. A., et al. 2024, *ApJ*, 966, 176
- Ziparo, F., Gallerani, S., Ferrara, A., & Vito, F. 2022, *MNRAS*, 517, 1086